Geomechanics and Engineering, *Vol. 23, No. 2 (2020) 139-149*
DOI: https://doi.org/10.12989/gae.2020.23.2.139

Effect of water content on near-pile silt deformation during pile driving using PIV technology

Tong Jiang, Lijin Wang*, Junran Zhang, Hang Jia and Jishun Pan

Henan Province Key Laboratory of Geomechanics and Structural Engineering, North China University of Water Resources and Electric Power, Zhengzhou, Henan 450045, China

(Received May 26, 2020, Revised August 2, 2020, Accepted September 27, 2020)

Abstract. Piles are widely used in structural foundations of engineering projects. However, the deformation of the soil around the pile caused by driving process has an adverse effect on adjacent existing underground buildings. Many previous studies have addressed related problems in sand and saturated clay. Nevertheless, the failure mechanism of pile driving in unsaturated soil remains scarcely reported, and this issue needs to be studied. In this study, a modeling test system based on particle image velocimetry (PIV) was developed for studying deformation characteristics of pile driving in unsaturated silt with different water contents. Meanwhile, a series of direct shear tests and soil-water characteristic curve (SWCC) tests also were conducted. The test results show that the displacement field shows an apparent squeezing effect under the pile end. The installation pressure and displacement field characteristics are sensitive to the water content. The installation pressure is the largest and the total displacement field is the smallest, for specimens compacted at water content of 11.5%. These observations can be reasonably interpreted according to the relevant unsaturated silt theory derived from SWCC tests and direct shear tests. The variation characteristics of the soil displacement field reflect the macroscopic mechanical properties of the soil around the pile.

Keywords: particle image velocimetry (PIV); model test; unsaturated; pile driving; displacement field; soil-water characteristic curve

1. Introduction

Silt is widely distributed in the Henan area in China and is convenient to use for highway construction projects. Owing to the poor engineering characteristics of silt (Ahmadi-Naghadeh 2019), a natural silt foundation does not meet the requirements of foundation strength and deformation. Therefore, a pile foundation is used for reinforcement that effectively reduces settlement. However, the strong disturbance of the surrounding soil caused by the driving process will have an adverse impact on the existing buildings. Extensive research has been conducted on the pile-driving process in saturated soil subgrade using different methodological approaches, including scale models (Liu *et al.* 2011, Al-Omari *et al.* 2016, Fattah *et al.* 2017, Al-abboodi *et al.* 2020), numerical simulations (Ekanayake 2013, Cyril *et al.* 2019, Hyodo *et al.* 2019, Jeon *et al.* 2020, Yuan *et al.* 2020), theoretical calculations (Masoumi *et al.* 2007, Li *et al.* 2020), and field tests (Gao *et al.* 2018). Most previous studies focused on pile driving in sand, transparent soil, and saturated clay. In recent years, some studies have been published on the influence of unsaturation in engineering problems such us bearing capacity of foundations. Lalicata *et al.* (2019) investigate the effects of saturation and unsaturation on the behaviour of laterally loaded piles. Most of the research focuses on the pile bearing capacity, but only a few studies the distribution and variation trend of the soil displacement field around the unsaturated subgrade during the pile driving process. Moreover, the influence of suction on pile-soil action mechanism in unsaturated subgrade is still unclear.

Particle image velocimetry (PIV) designed originally for fluid mechanics is widely used to measure soil deformation (Yuan *et al.* 2012, Zhang *et al.* 2019), and the strain and displacement fields of a sample surface can be accurately determined using PIV technology (Qi *et al.* 2017, Yuan *et al.* 2017, You and Chen 2018). In recent years, the PIV technology has been applied to unsaturated soils. Azmatch *et al.* (2008) studied the growth and microscopic mechanism of frozen soil ice lens based on PIV technology using Devo clay labeled with fluorescent powder aqueous solution, and pointed out that the consolidation phenomenon of frozen soil was related to the change of pore water pressure. Using PIV and DIC techniques, Li *et al.* (2019) studied the development of displacement direction and strain concentration during tension. In summary, PIV technology has been developed in the measurement of unsaturated soil stress-displacement/strain characteristics.

The embankment soil in the Henan area is mostly unsaturated owing to the subgrade height above the water table. Therefore, the study of unsaturated soil is an urgent need for subgrade soil (Wang *et al.* 2020). Matric suction is the core of unsaturated soil research (Zhang *et al.* 2016, Gao *et al.* 2019, Xin *et al.* 2020, Zhang *et al.* 2020), and the soil-water characteristic curve (SWCC), which characterizes the relationship between matric suction and

*Corresponding author, Ph.D.
E-mail: 201300804@stu.ncwu.edu.cn

ISSN: 2005-307X (Print), 2092-6219 (Online)

water content, is essential (Fredlund and Xing 1994, Bordoni *et al.* 2017). Many studies have addressed the influence of different factors on SWCCs and proposed methods for their prediction (Sun *et al.* 2007, Jayanth *et al.* 2012, Bareither and Benson 2013, Zhou *et al.* 2019). The SWCC is of considerable significance to solve the problem of unsaturated soil and can quickly provide useful parameters for geotechnical engineering projects.

In order to further clarify the internal mechanism of pile squeezing effects and the influence of suction on pile bearing capacity in unsaturated subgrade. A modeling test system based on PIV was developed for studying the process of single pile driving in unsaturated silt. A charge-coupled device (CCD) high-speed camera and Davis8.0 series acquisition software were used to record images throughout the entire testing period, a loading system was used to measure the installation pressure, and the post-processing software such as PIVview2C was used to obtain the displacement field distribution of soil around the pile. The deformation field of unsaturated silt around the pile was determined, and the mesoscopic silt deformation characteristics with variable water content were deeply analyzed. Direct shear tests and SWCC tests were conducted for studying the physical and water retention characteristics of unsaturated silt. The results are discussed in combination with test results of pile driving process.

2. Materials and methods

2.1 Experimental setup

2.1.1 SWCC testing apparatus

As shown in Fig. 1, the Geotechnical Consulting and Testing Systems (GCTS) SWCC apparatus is a set of unsaturated soil testing equipment used to obtain the soil SWCC. The pore water pressure is applied from the bottom through the high-air entry disk, and the pore air pressure is applied from the top cap. The matric suction of the specimen is controlled by axial translation (Hilf 1956, Fattah *et al.* 2017).

2.1.2 Direct shear testing apparatus

An SDJ-1 three-speed electric direct shear apparatus was used to measure soil shear strength. The controllable shear speeds are 0.02, 0.8, and 2.4 mm/min. The maximum vertical load is 400 kPa, and the maximum horizontal shear force is 1.2 kN.

2.1.3 PIV model testing apparatus

The automatic static pile-driving device with an image capture system is shown in Fig. 2. This apparatus consists of two systems: a loading system and an image capture system. The loading system is a CMT4000 electronic universal testing machine developed by the American Meester Company, includes loading equipment and a data acquisition system, and is used to apply the pile pressure and measure the driving depth of the static pile. The load is imposed with a constant velocity displacement rate (0 ~ 10 mm/min), and the pile driving speed in the test was 10 mm/min. The load data is determined from a loading cell with the capacity of 160 N, the accuracy of 0.03% Full Scale (FS), and the resolution of 0.001 N. Displacement is determined from measurements using a linear variable differential transducer (LVDT) with the capacity of 100 mm, the accuracy of 0.1% Full Scale (FS), and the resolution of 0.001 mm. Both the load cell and LVDT collect information simultaneously during testing. Specimen deformation is therefore performed synergistically with the load applied by the loading system.

Fig. 1 GCTS SWCC experimental setup

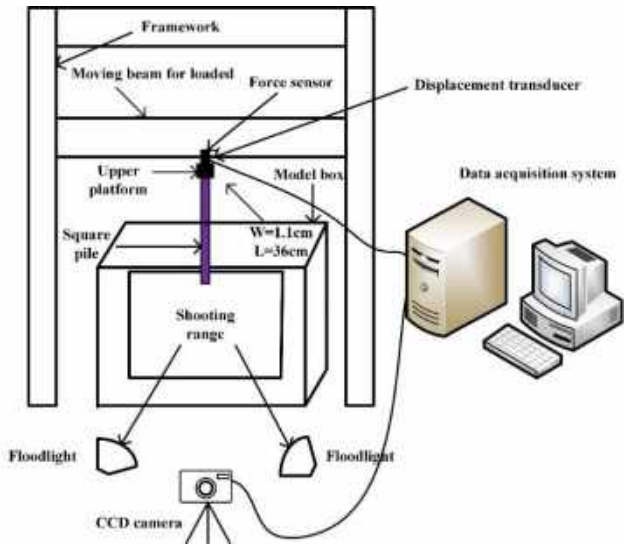

Fig. 2 PIV experimental setup

The image capture system consists of floodlights, CCD high-speed cameras, Davis 8.3.0 series software, and post-processing software, including PIVview2C. The range of the photographed specimens was 38.5 × 38.5 cm. The outer boundary size of the upper opening of the model box was 35 × 20 cm, the wall thickness was 1.0 cm, and the height was 30 cm. The model pile made of a steel plate was square with a length of 36 cm and a width of 1.1 cm, and the pile end was flat, as shown in Fig. 2. According to Qi *et al.* (2015), the slenderness ratio for buckling is mainly affected by the material and the slenderness ratio of the pile. The pile used in this study is a rigid pile with a moderate slenderness ratio, so it is not easy to occur buckling

Table 1 Physical and mechanical properties of the silt

Specific gravity, G_s	Liquid limit, w_L (%)	Plastic limit, w_P (%)	Plastic index, I_p	Maximum dry density, ρ_d(g/cm^3)	Optimum Water contents, w_{opt} (%)
2.7	25	19	6	1.72	12.7

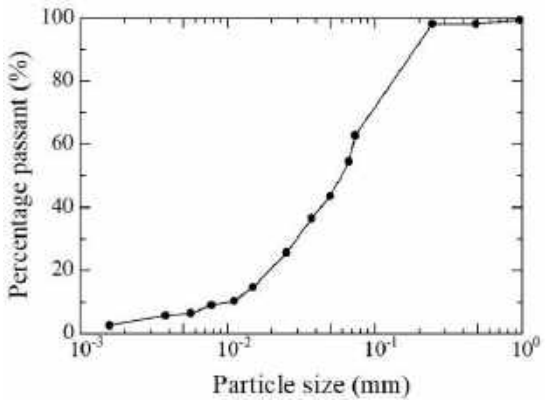

Fig. 3 Particle size distribution of Yudong silt

Table 2 Suction paths

Path type	Suction path
Drying	1 kPa→10 kPa→20 kPa→40 kPa→80 kPa→160 kPa→320 kPa

instability failure. The relative buckling length of the rigid pile is not considered in this study, which can be theoretically calculated in future research. According to Bolton *et al.* (1999), when the pile diameter is 20 times higher than the average soil diameter, and the distance between the pile and the boundary is at least ten times greater than the pile diameter, the particle size effect and boundary effect are tolerable. Both of the above conditions are met in this model test.

2.1.4 Physical and mechanical properties of silt

Soil samples were collected from Yudong in eastern Henan at a depth of ~3 m. The main physical and mechanical properties of the specimens are listed in Table 1. The liquid limit and plastic limit of the samples are 25% and 19%, respectively, and the the plasticity index of the silt is 6. As shown in Fig. 3, the silt particle content was up to 60%, and the soil specimen is sandy silt with a low liquid limit.

2.2 Testing program

2.2.1 Testing program for SWCC

The initial specimen size used in the tests was d_0=6.18 cm and h_0=2 cm. The water content (w) and dry density of the specimen were 12.7% and 1.55 g/cm^3, respectively. The specimen was then saturated using a vacuum pump.

As shown in Table 2, the SWCC test was conducted at net stress of 1 kPa. The specimen was first placed on the clay plate in the pressure chamber, and the desired air pressure was applied. The specimen was then applied with different matric suction to measure the SWCC along the dry path. After the specimen reached a balance with a given suction, it was removed from the GCTS unsaturated soil odometer. Its volume and water content were obtained by measuring its size and mass. The relationship between water content and matric suction can be obtained by integrating the experimental results of each suction balance.

Table 3 Direct shear test program for the unsaturated Yudong silt

Dry density, ρ_d (g/cm^3)	Initial water content, w_0 (%)	Normal stress, σ_v(kPa)
1.45	3.5	100, 200, 300, 400
	9.5	
	11.5	
	13.4	
	17.3	

Fig. 4 Model test specimen

2.2.2 Direct shear testing program

During sample preparation, the dry silt density was controlled at 1.45 g/cm^3, and water contents of 3.5%, 9.5%, 11.5%, 13.4%, and 17.3% were applied to five separate sample groups. As shown in Table 3, four specimens from each group were then applied with a normal vertical pressure of 100, 200, 300, and 400 kPa, respectively, for quick shear testing using a shear rate of 0.8 mm/min.

The time of direct shear test completed at this shear rate is the closest to the time of pile driving. And it is more convenient to explain the test mechanism of pile driving process with the change law of unsaturated silt cohesion obtained by direct shear test.

2.2.3 PIV Model testing program

Matric suction is an important parameter to study the engineering properties of unsaturated soil and is closely related to water content (Gu *et al.* 2019, Satyanaga and Rahardjo 2019). We therefore study the properties of unsaturated soil by controlling the water content to 3.5%, 9.5%, 11.5%, 13.4%, and 17.3%. The core emphasis of this study is to analyze the influence of water content on the displacement field of soil around the pile and installation pressure during pile driving in a silt foundation. A fixed dry density of 1.45 g/cm^3 was therefore applied. The dry soil quality of each group is consistent. After the soil sample is

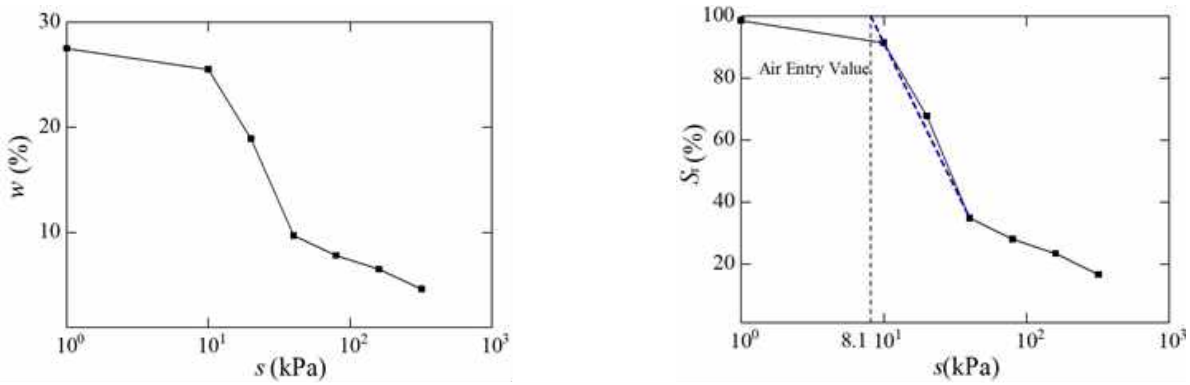

(a) *w*-*s* (b) S_r-*s*

Fig. 5 Soil-water characteristic curve of unsaturated Yudong silt with an initial dry density of 1.55 g/cm^3

prepared according to the target water content, it is screened firstly and then placed in the moisturizing tank for 24 hours to make it evenly mixed. After distributing the soil according to the required total soil, it is divided into three layers and compacted at a certain height, so as to ensure that the dry density of each group is consistent. A prepared specimen with the water content of 9.5% is shown in Fig. 4.

The PIV measurement system and loading system were turned on and the camera was calibrated with a special calibration board. After calibration, the camera frequency and photo number of the PIV measurement system were set. To record the entire pile-driving process, the pile loading rate was set to 10 mm/min, and the photo collection frequency of the high-speed camera was one sheet/s. The loading system and the image capture system are controlled by two people, and the test is started at the same time with a stopwatch to ensure that the test can be synchronized. After the test, all pictures were converted to grayscale images and imported into the computer programs PIVview2C and tecplot10 for PIV analyses. The soil deformation at different stages was determined by comparing the pictures at the beginning and end of each stage.

3. Results

3.1 SWCC test results

The obtained SWCCs are shown in Fig. 5. Water content (w) and degree of saturation (S_r) decrease with increasing suction (s). The relationship between water content (w) and suction (s) is shown in Fig. 5(a). When s is relatively small, the water content decreases slowly with increasing suction, and the slope of the curve is lower. When s reaches 10 kPa, pore water in the specimen is discharged in large quantities, the water content decreases rapidly, and the slope of the curve abruptly increases. When s is greater than 40 kPa, pore water continues to be discharged, and the water content decreases gradually. When s reaches 320 kPa, the water content is already very low. The shape of the SWCC is closely related to the basic silt properties. The clay content of silt is low and the water retention capacity is not strong, so it is reflected that the slope of the soil-water characteristic curve is steep and the residual water content is low.

The relationship between the degree of saturation (S_r) and the suction (s) is shown in Fig. 5(b). The saturation curve can be divided into three distinct stage characteristics, which are the boundary effect section, the transition section, and the unsaturated residual section. In the boundary effect stage, the variation of suction value is small, and the water in the soil sample is discharged by gravity. In the transition stage, the water in the soil sample is largely discharged with increasing suction, the saturation decreases, and the final reduction rate decreases. As the saturation continues to decrease, the liquid phase in the soil gradually ceased to be continuous. At this time, the soil gradually entered the unsaturated residual section, and the pore water changed from gravity water to combined water and capillary water. The silt used in this paper has a relatively large particle size and large pore size. Therefore, as shown in Fig. 5(b), the air entry value is 8.1 kPa, pore water can be discharged under small matric suction conditions (Wang and Li 2015). When s reaches 320 kPa, the drainage rate decreases, and the soil saturation is already low at this time (Zhang *et al.* 2018, Zhang *et al.* 2019). Tao *et al.* (2018) tested the soil-water characteristic curves of various soils. The silt air entry value is relatively low and the water retention capacity is weak, which is consistent with the experimental results in this paper.

3.2 Direct shear test results

The relationship between vertical stress and shear strength of silt with different water contents is shown in Fig. 6. When the water content is low, the shear strength of soil increases with increasing water content. When water content reached 11.5%, the shear strength of soil began to decrease with increasing water content. The slope of the strength envelope of silt with different water contents is essentially the same, and the angle of internal friction ranges between 20° and 23°. Silt cohesion initially increases with increasing water content and then decreases, as shown in Fig. 7. Cohesion is the largest (i.e., 39.4 kPa) for the silt specimens compacted with the water content of 11.5%. These findings are consistent with the results of Wei *et al.* (2019). From the above test results, it can be seen that the effect of water content on shear strength is mainly through reducing or enhancing cohesion, and the effect of water

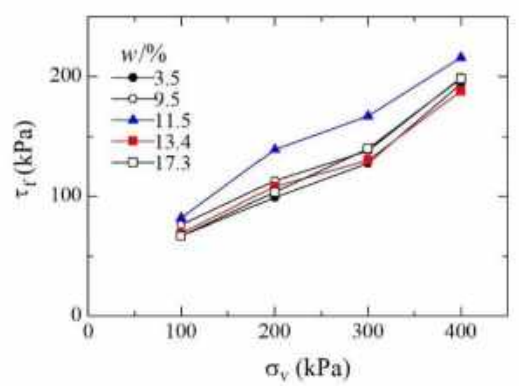

Fig. 6 Relationship between the vertical stress and the shear strength of silts with different water content

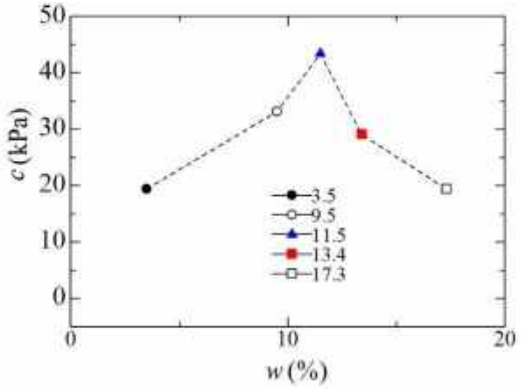

Fig. 7 Relationship between the silt cohesion and the water content

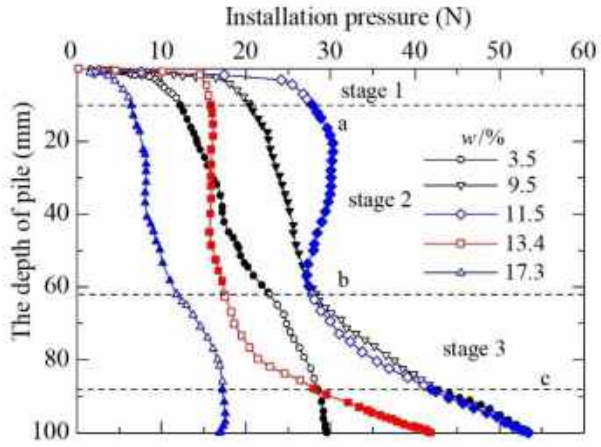

Fig. 8 Relationships between the pile installation pressure and the depth during pile driving

content on the angle of internal friction is less.

Gao *et al.* (2020) pointed out that the shear strength of different soil types over a wide suction range can be broadly classified into three groups. For sand, the shear strength usually increases with increasing suction to a marked peak value and then decreases sharply to a fairly constant value. For silt or silty clay, as the suction increases, the shear strength increases to a fairly constant value or a maximum. For some silty clay or clay, the shear strength always increases with the increasing suction. The soil of the paper is sandy silt with a low liquid limit and its engineering properties are between silt and sand. Therefore the shear strength of the soil increases and then decreases with increasing water content.

3.3 Relationship between the installation pressure P and the depth of pile H with different water contents

The relationship between the installation pressure P and the pile depth H is shown in Fig. 8. When the water content is 3.5% and 17.3%, the P-H curve morphologies are mostly the same, both showing an upward convex trend. When the water content is 9.5%, 11.5%, and 13.4%, the P-H curve morphologies are also essentially the same, but tend to be convex first and then concave. The P-H curve changes the most significant when the water content is 11.5%. The P-H curve can be roughly divided into three stages based on its morphology characteristics. The relationship curve between P and H is therefore related to the water contents of the unsaturated silt.

In the first stage, there is a linear phase in the P-H curve, and P increases linearly with increasing H. It is consistent with the well-known increment of preconsolidation stress in unsaturated soils (Gens 2010). According to Lalicata *et al.* (2019), this stage cannot be found in saturated condition. Then, as the pile depth increases, the soil around the pile undergoes plastic deformation, and P continues to increase, but the derivative of P decreases rapidly. P initially increases with increasing water content and then decreases, and is the largest when the water content is 11.5%. In the second stage, the soil under the pile end continues to be compressed. With increasing pile depth, P does not increase significantly, or even remains unchanged or decreased. The stress of the soil under the pile end exceeds its shear strength, and it can be considered that the soil at this stage has been damaged. These observations are similar to those of Kong *et al.* (2015) and can be called the destruction stage. For specimens compacted at 9.5%, 11.5% and 13.4% water content, the inflection point of the curve is more obvious, as shown in Fig. 8; For specimens compacted at 3.5% and 17.3% water content, strain hardening occurs in the soil when the pile depth is relatively large.

3.4 Deformation field of soil around the pile during pile driving

Comparative analysis was performed by comparing pictures recorded at the beginning and end of each stage PIVview2C and tepclot 10 software were then used to generate a cloud map and contour map, respectively. The displacement contour maps are given immediately after loading.

3.4.1 Specimens compacted with 3.5% and 17.3% water content

The comprehensive analysis of specimens compacted at water contents of 3.5% and 17.3% (Figs. 9 and 10) show that the displacement field characteristics of the soil around the pile are similar and can be roughly divided into two stages by the morphological characteristics of the P-H curve.

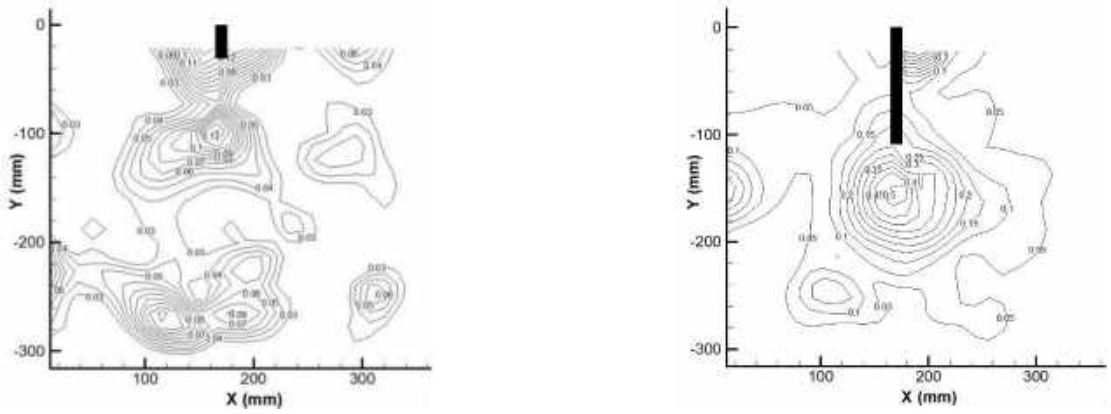

(a) Displacement field in the first stage (b) Displacement field in the second stage

Fig. 9 Displacement field of soil around the pile during different stages (w=3.5%)

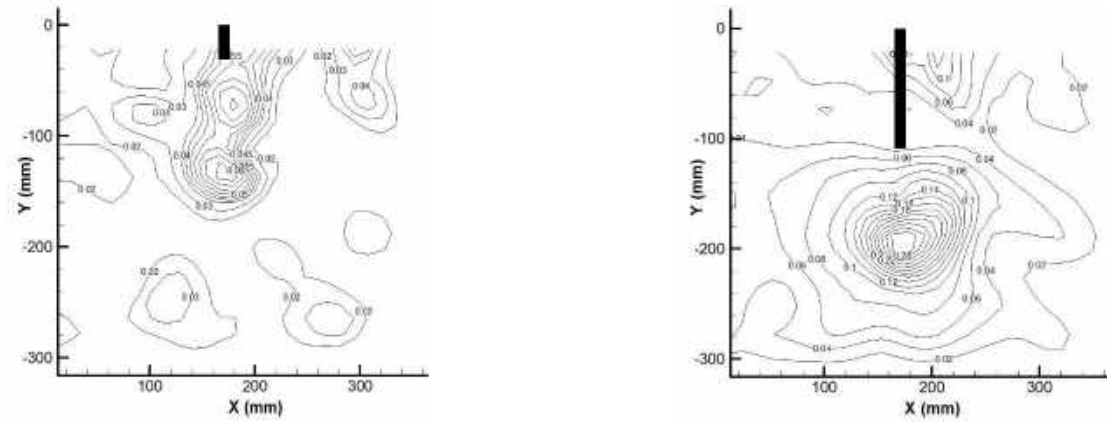

(a) Displacement field in the first stage (b) Displacement field in the second stage

Fig. 10 Displacement field of soil around the pile during different stages (w=17.3%)

In the first stage, at a depth of ~10 mm, the upper soil is continuously disturbed, and its displacement changes greatly. With increasing pile depth, the soil under the pile end is continuously compressed, the soil force is continuously strengthened, and the soil displacement field increases significantly. In the figure, it appears as two sets of elliptical rings that are concentratedly distributed in the upper soil and the soil under the pile end. Soil disturbance on both sides of the static pile is essentially the same, showing a fundamental symmetric trend. The maximum displacement field appears below the pile end.

In the second stage, at a depth of ~88 mm, the squeezing effect becomes more apparent with increasing pile driving depth and the dense disturbance area moves down. As shown in Figs. 9 and 10, a set of displacement contours in the shape of an elliptical ring appears below the pile end. The distribution of the contours is more concentrated, and the values are larger than other situations. The displacement field is essentially symmetrically distributed on both sides of the pile. The soil disturbance around the pile due to large deformation and extrusion is more concentrated and distributed. The maximum displacement field also appears below the pile end. Due to the destruction of soil around the pile, the maximum displacement field increased significantly compared with the previous stage.

3.4.2 Specimens compacted with 9.5% ,11.5% and 13.4% water content

The comprehensive analysis of specimens compacted at water contents of 9.5%, 11.5%, and 13.4% (Figs. 11, 12, and 13) show that the displacement field characteristics of the soil around the pile are similar and can be roughly divided into three stages in accordance with the morphological characteristics of the *P-H* curve. In the first stage, at a depth of ~10 mm, under the pile end, the soils is compressed and the displacement field is shown as an independent elliptical ring in the figure. Soil disturbance on both sides of the pile is essentially the same, showing a essential symmetric trend. The maximum displacement field appears below the pile end.

In the second stage, at a depth of ~62 mm, the soil under the pile end is compressed and the displacement field moves down, presenting a symmetrical trend of gradual downward movement. The soil under the pile end is damaged when the stress exceeds its shear strength. The soil disturbance around the pile due to large deformation and extrusion is more concentrated and distributed. The maximum displacement field also appears below the pile end.

In the third stage, at a depth of ~88 mm, according to the morphological characteristics of the *P-H* curve, this

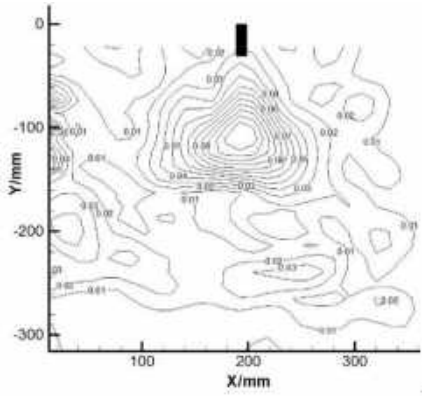

(a) Displacement field in the first stage

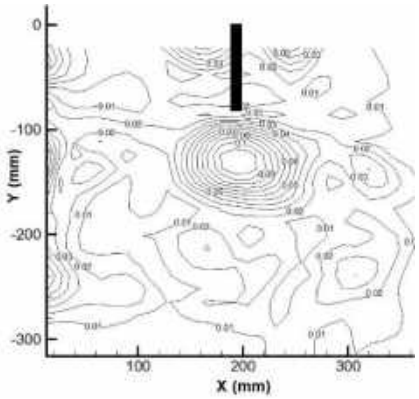

(b) Displacement field in the second stage

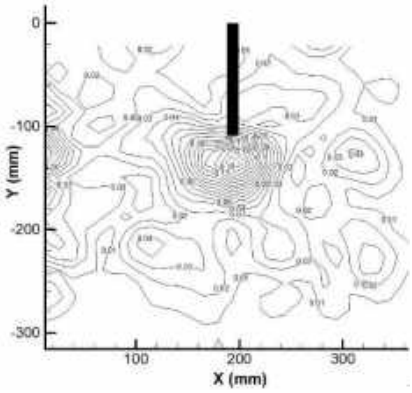

(c) Displacement field in the third stage

Fig. 11 Displacement field of soil around the pile during different stages (w=9.5%)

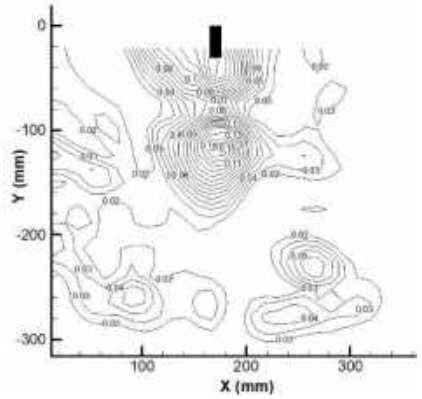

(a) Displacement field in the first stage

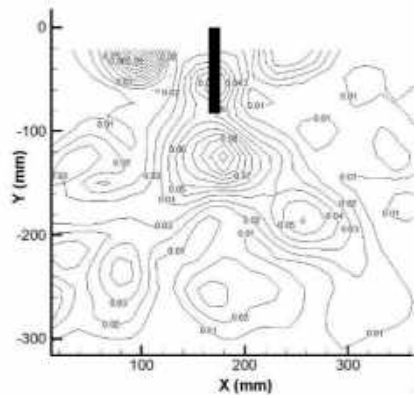

(b) Displacement field in the second stage

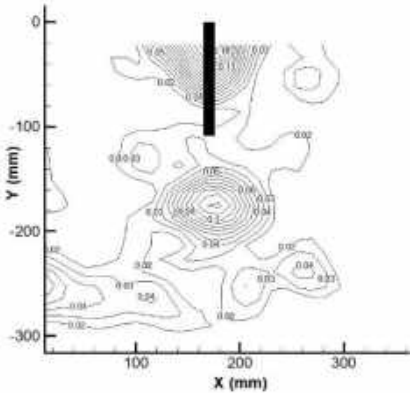

(c) Displacement field in the third stage

Fig. 12 Displacement field of soil around the pile during different stages (w=11.5%)

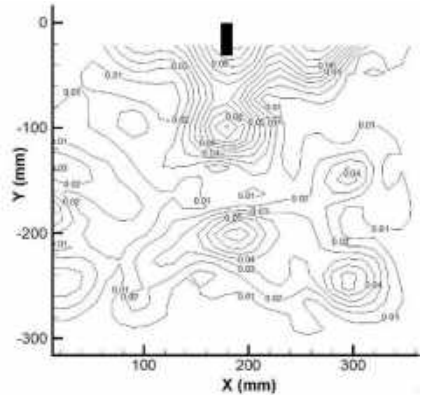

(a) Displacement field in the first stage

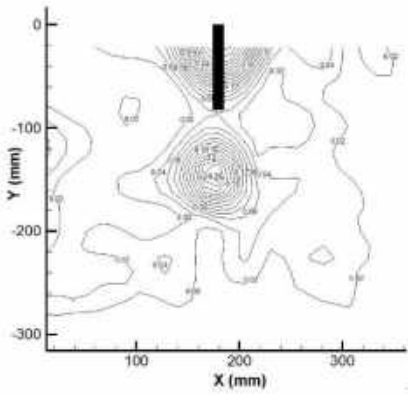

(b) Displacement field in the second stage

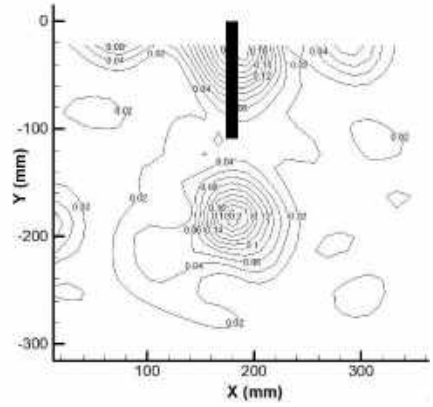

(c) Displacement field in the third stage

Fig. 13 Displacement field of soil around the pile during different stages (w=13.4%)

increasing pile depth, the upper soil is continuously disturbed, and the soil under the pile end is compressed, resulting in larger deformation. With increasing pile depth, the distribution of displacement contour is more concentrated, that is, the distribution of soil around the pile caused by large deformation and extrusion becomes more concentrated, while the soil deformation in other regions does not change significantly.

4. Discussion

Comparative analyses are shown in Figs. 6 and 8. In the first stage, under the same settlement depth condition, the installation pressure (Fig. 8) and shear strength (Fig. 6) both first increase and then decrease with increasing water content. The water content of the silt has a significant influence on the relationship curve between the installation pressure P and the pile depth H. For unsaturated soils, the change of microstructure with water content should be considered (Trabelsi *et al.* 2018, Xin *et al.* 2020). Most of the water is stored inside aggregate pores at low water contents, and it is very difficult to form liquid bridges (Gens and Alonso 1992). The soil shear strength depends mainly on the liquid bridges among particles. When w is less than the optimum water content, the liquid bridges form gradually with increasing water content, thus the shear strength increases with increasing water content. When the water content increases up to the optimum water content,

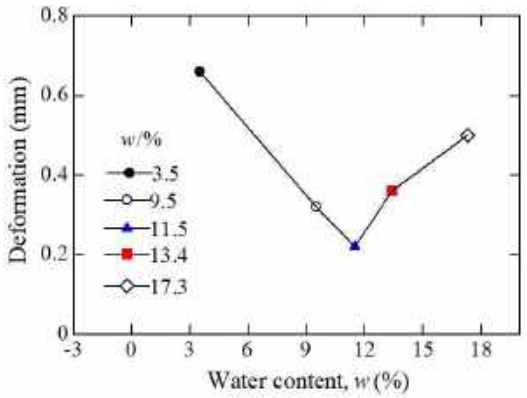

Fig. 14 The maximum total deformation of samples with different water contents

the liquid bridges appear at most contact points of particles. The liquid bridges among particles will disappear gradually with further increasing water content, resulting in a decrease in the shear strength. Therefore, the installation pressure is the maximum for specimens compacted at water content of 11.5%.

The total deformation field under each condition was obtained by comparing pictures recorded at the end of the experiment with the reference picture taken before testing under different water contents conditions, as shown in Fig. 14. The total deformation first decreases and then increases with increasing water content and is the smallest near the optimal water content. The deformation variables of the

Fig. 15 Soil remains upright after the pile is pulled out

samples with five different water contents are 0.66, 0.32, 0.22, 0.36, and 0.50 mm, respectively. As shown in Figs. 7 and 14, the displacement field of the soil around the pile is related to the cohesion of the unsaturated silt during pile driving. When the water content is exceedingly high or low, the effective surface tension on the shrink film of the gas-water interface between the powder particles will decrease, resulting in decreased cohesion. The relationship between suction and water content is shown in Fig. 5(a). When the water content is in the transition zone of the SWCC, the water and air in the soil are connected and belong to a double open system. The reaction force of the surface tension on the shrink film of the gas-water interface acts on the soil particles, causing compressive stress on the soil particles, resulting in increased soil cohesion. When the water content is close to optimal, the cohesion of the unsaturated silt is the largest, the self-stability is strong, and the soil around the pile is less disturbed during the pile-driving process, therefore reducing the displacement field. In other words, the deformation field characteristics of the soil around the pile with different water contents are closely related to the cohesion of the unsaturated silt. Variation of the PIV deformation field of the soil particles also reflects the macroscopic soil mechanical properties.

The displacement contour of unsaturated soil around the pile during pile driving indeed differs from the test results of a pile in dry sand published in the literature. In particular, because unsaturated silt has a certain suction or cohesion, the soil around the pile end keeps the soil upright after the pile is pressed into the soil. A photograph that shows how the model soil remains upright after the pile is pulled out (e.g., w = 11.5%) is shown in Fig. 15.

5. Conclusions

A series of comparative model tests based on particle image velocimetry was performed, and a model test system of static pile driving was developed to study the deformation characteristic of static pile driving in unsaturated silt with different water contents. The main conclusions are as follows.

• Because the air entry value of silt is small, the water content and saturation start to decrease when the suction is very small. When the water content is in the transition region of the SWCC, water content and saturation decrease rapidly. Silt has poor water retention capability, so when s is high, the water content is small.

• In the process of pile driving, as the depth of the driving pile increases, there is a linear phase in the load-displacement relationship, which cannot be found in saturated condition. And then the soil will undergo plastic deformation. Finally, when the stress on the soil exceeds its shear strength, the soil is damaged. For specimens compacted at water content of 9.5%, 11.5% and 13.4%, the damage stage is more obvious; For specimens compacted at water content of 3.5% and 17.3%, strain hardening occurs in the soil when the pile depth is relatively large. The water content of silt has an important influence on the relationship curve of *P-H*, and the installation pressure is the largest for specimens compacted at water content of 11.5%.

• In the process of pile driving, the displacement fields on both sides of the pile are essentially symmetrically distributed. With increasing pile depth, the densely disturbed area moves downward, and the concentrated distribution of the disturbed area caused by large deformation and extrusion becomes more apparent. In this process, the upper soil is continuously disturbed, the soil under the pile end is continuously compressed, and the maximum displacement occurs under the pile end. When the damage is reached, the deformation of soil around the pile is more significant.

• The total deformation first decreases and then increases with increasing water content. When the specimen is compacted with optimal water content, the unsaturated silt has the largest cohesion and strong self-stability. The soil around the pile is therefore less disturbed during pile driving, resulting in the smallest deformation value. The results show that variation of the PIV deformation field of the soil particles reflects the macroscopic soil mechanical properties.

Acknowledgments

This study is financially supported by the National Natural Science Foundation of China (Grant No. 41602295), the Foundation for University Key Teacher by the Ministry of Education of Henan Province (Grant No. 2020GGJS-094), the Key Scientific Research Projects of Colleges and Universities in Henan Province (Grant No. 21A410002), and the Doctoral Student Innovation Foundation of NCWU.

References

Ahmadi-Naghadeh, R. and Toker, N.K. (2019), "A new isotropic specimen preparation method from slurry for both saturated and unsaturated triaxial testing of a low-plasticity silt", *Geotech. Test. J.*, **42**(4), 854-879. https://doi.org/10.1520/GTJ20170269.

Al-abboodi, I., Sabbagh, T.T. and Al-salih, O. (2020), "Response of passively loaded pile groups-an experimental study", *Geomech. Eng.*, **20**(4), 333-343. https://doi.org/10.12989/gae.2020.20.4.333.

Al-Omari, R.R., Al-Azzawi, A.A. and AlAbbas, K.A. (2016), "Behavior of piled rafts overlying a tunnel in sandy soil",

Geomech. Eng., **10**(5), 599-615. https://doi.org/10.12989/gae.2016.10.5.599.

Azmatch, T.F., Arenson, L.U., Sego, D.C. and Biggar, K.W. (2008), "Measuring ice lens growth and development of soil strains during frost penetration using particle image velocimetery (GeoPIV)", *Proceedings of the 9th International Conference on Permafrost*, Fairbanks, Alaska, June-July.

Bareither, C.A. and Benson, C.H. (2013), "Evaluation of Bouwer-Rice large-particle correction procedure for soil water characteristic curves", *Geotech. Test. J.*, **36**(5), 680-694. https://doi.org/10.1520/GTJ20130013.

Bolton, M.D., Gui, M.W., Garnier, J., Corte, J.F., Bagge, G., Laue, J. and Renzi, R. (1999), "Centrifuge cone penetration tests in sand", *Géotechnique*, **49**(4), 543-552. https://doi.org/10.1680/geot.1999.49.4.543.

Bordoni, M., Bittelli, M., Valentino, R., Chersich, S. and Meisina, C. (2017), "Improving the estimation of complete field soil water characteristic curves through field monitoring data", *J. Hydrol.*, **552**, 283-305. https://doi.org/10.1016/j.jhydrol.2017.07.004.

Cyril, P.A., Kok, S.T., Song, M.K., Chan, A., Wong, J.Y. and Choong, W.K. (2019), "Smooth particle hydrodynamics for the analysis of stresses in soil around Jack-in pile", *Eur. J. Environ. Civ. Eng.*, 1-27. https://doi.org/10.1080/19648189.2019.1649198.

Ekanayake, S.D., Liyanapathirana, D.S. and Leo, C.J. (2013), "Influence zone around a closed-ended pile during vibratory driving", *Soil Dyn. Earthq. Eng.*, **53**, 26-36. https://doi.org/10.1016/j.soildyn.2013.06.005.

Fattah, M.Y., Salim, N.M. and Irshayyid, E.J. (2017), "Determination of the soil-water characteristic curve of unsaturated bentonite-sand mixtures", *Environ. Earth Sci.*, **76**(5), 201. https://doi.org/10.1007/s12665-017-6511-2.

Fattah, M.Y., Zabar, B.S. and Mustafa, F.S. (2017), "Vertical vibration capacity of a single pile in dry sand", *Mar. Georesour. Geotechnol.*, **35**(8), 1111-1120. https://doi.org/10.1080/1064119X.2017.1294219.

Fredlund, D.G. and Xing, A. (1994), "Equations for the soil-water characteristic curve", *Can. Geotech. J.*, **31**(4), 521-532. https://doi.org/10.1139/t94-061.

Gao, G.Y., Zhuang, Y., Wang, K.Y. and Chen, L. (2018), "Influence of Benoto bored pile construction on nearby existing tunnel: A case study", *Soils Found.*, **59**(2), 544-555. https://doi.org/10.1016/j.sandf.2018.11.006.

Gao, Y., Sun, D.A. and Zhu, Z.C. (2019), "Hydromechanical behavior of unsaturated soil with different initial densities over a wide suction range", *Acta Geotechnica*, **14**(2), 417-428. https://doi.org/10.1007/s11440-018-0662-5.

Gao, Y., Sun, D.A., Zhou, A.N. and Li, J. (2020), "Predicting shear strength of unsaturated soils over wide suction range", *Int. J. Geomech.*, **20**(2), 04019175. https://doi.org/10.1061/(ASCE)GM.1943-5622.0001555.

Gens, A. (2010), "Soil-environment interactions in geotechnical engineering", *Géotechnique*, **60**(1), 3-74. https://doi.org/10.1680/geot.9.P.109.

Gens, A. and Alonso, E.E. (1992), "A framework for the behaviour of unsaturated expansive clays", *Can. Geotech. J.*, **29**(6), 1013-1032. https://doi.org/10.1139/t92-120.

Gu, T.F., Wang, J.D., Wang, C.X., Bi, Y.Q., Guo, Q.Y. and Liu, Y.M. (2019), "Experimental study of the shear strength of soil from the Heifangtai platform of the loess plateau of China", *J. Soils Sediments*, **19**(10), 3463-3475. https://doi.org/10.1007/s11368-019-02303-9.

Hilf, J.W. (1956), "An investigation of pore-water pressure in compacted cohesive soils", Technical Memorandum No. 654, U.S. Department of the Interior, Bureau of Reclamation, Design and Construction Division, Denver, Colorado, U.S.A.

Hyodo, J., Shiozaki, Y., Tamari, Y., Ozutsumi, O. and Ichii, K. (2019), "Modeling of pile end resistance considering the area of influence around the pile tip", *Geomech. Eng.*, **17**(3), 289-296. https://doi.org/10.12989/gae.2019.17.3.289.

Jayanth, S., Iyer, K. and Singh, D. (2012), "Influence of drying and wetting cycles on SWCCs of fine-grained soils", *J. Test. Eval.*, **40**(3), 376-386. https://doi.org/10.1520/JTE104184.

Jeon, Y.J., Jeon, S., Jeon, S.J. and Lee, C.J. (2020), "Study on the behaviour of pre-existing single piles to adjacent shield tunnelling by considering the changes in the tunnel face pressures and the locations of the pile tips", *Geomech. Eng.*, **21**(2), 187-200. https://doi.org/10.12989/gae.2020.21.2.187.

Kong, G.Q., Cao, Z.H., Zhou, H. and Sun, X.J. (2015), "Analysis of piles under oblique pullout load using transparent-soil models", *Geotech. Test. J.*, **38**(5), 725-738. https://doi.org/10.1520/GTJ20140109.

Lalicata, L.M., Desideri, A., Casini, F. and Thorelc, L. (2019), "Experimental observation on laterally loaded pile in unsaturated silty soil", *Can. Geotech. J.*, **56**(11), 1545-1556. https://doi.org/10.1139/cgj-2018-0322.

Li, C., Zou, J.F. and Li, L. (2020), "A novel approach for predicting lateral displacement caused by pile installation", *Geomech. Eng.*, **20**(2), 147-154. https://doi.org/10.12989/gae.2020.20.2.147.

Li, H.D., Tang, C.S., Cheng, Q., Li, S.J., Gong, X.P. and Shi, B. (2019), "Tensile strength of clayey soil and the strain analysis based on image processing techniques", *Eng. Geol.*, **253**, 137-148. https://doi.org/10.1016/j.enggeo.2019.03.017.

Liu, J.Y., Yuan, B.X., Mai, V.T. and Dimaano, R. (2011), "Optical measurement of sand deformation around a laterally loaded pile", *J. Test. Eval.*, **39**(5), 754-759. https://doi.org/10.1520/JTE103313.

Masoumi, H., Degrande, G. and Lombaert, G. (2007), "Prediction of free field vibrations due to pile driving using a dynamic soil-structure interaction formulation", *Soil Dyn. Earthq. Eng.*, **27**(2), 126-143. https://doi.org/10.1016/j.soildyn.2006.05.005.

Qi, C.G., Chen, Y.H., Wang, X.Q. and Zuo, D.J. (2015), "Physical modeling experiment on buckling of slender piles in transparent soil", *Chin. J. Rock Mech. Eng.*, **34**(4), 838-848.

Qi, C.G., Zheng, J.H. and Zuo, D.J. (2017), "Measurement on soil deformation caused by expanded-base pile in transparent soil using particle image velocimetry (PIV)", *J. Mountain Sci.*, **14**(8), 1655-1665. https://doi.org/10.1007/s11629-016-4025-0.

Satyanaga, A. and Rahardjo, H. (2019), "Unsaturated shear strength of soil with bimodal soil-water characteristic curve", *Géotechnique*, **69**(9), 828-832. https://doi.org/10.1680/jgeot.17.P.108.

Sun, D.A., Sheng, D.C. and Sloan, S.W. (2007), "Elastoplastic modeling of hydraulic and stress-strain behavior of unsaturated soils", *Mech. Mater.*, **39**(3), 212-221. https://doi.org/10.1016/j.mechmat.2006.05.002.

Tao, G.L., Chen, Y., Kong, L.W., Xiao, H.L., Chen, Q.S. and Xia, Y.X. (2018), "A simple fractal-based model for soil-water characteristic curves incorporating effects of initial void ratios", *Energies*, **11**(6), 1419. https://doi.org/10.3390/en11061419.

Trabelsi, H., Romero, E. and Jamei, M. (2018), "Tensile strength during drying of remoulded and compacted clay: The role of fabric and water retention", *Appl. Clay Sci.*, **162**, 57-68. https://doi.org/10.1016/j.clay.2018.05.032.

Wang, L., Zhou, A.N., Xu, Y.F. and Xia, X.H. (2020), "Consolidation of unsaturated composite ground reinforced by permeable columns", *Comput. Geotech.*, **125**, 103706. https://doi.org/10.1016/j.compgeo.2020.103706.

Wang, X.L. and Li, J.C. (2015), "A novel liquid bridge model for estimating SWCC and permeability of granular material", *Powder Technol.*, **275**, 121-130. https://doi.org/10.1016/j.powtec.2015.01.044.

Wei, Y.J., Wu, X.L., Xia, J.W., Miller, G.A., Cai, C.F., Guo, Z.L. and Arash, H. (2019), "The effect of water contents on the shear strength characteristics of granitic soils in South China", *Soil Till. Res.*, **187**, 50-59. https://doi.org/10.1016/j.still.2018.11.013.

Xin, L., Zhou, A.N., Li, J. and Feng, S.J. (2020), "Reproducing micro X-ray computed tomography (microXCT) observations of air–water distribution in porous media using revised pore-morphology method", *Can. Geotech. J.*, **57**(1), 149-156. https://doi.org/10.1139/cgj-2018-0662.

Xin, L., Zhou, A.N., Shen, S.L., Li, J. and Sheng, D.C. (2020), "A micro-mechanical model for unsaturated soils based on DEM", *Comput. Meth. Appl. Mech. Eng.*, **368**, 113183. https://doi.org/10.1016/j.cma.2020.113183.

You, Z.J. and Chen, Y.L. (2018), "The use of tactile sensors and PIV analysis for understanding the bearing mechanism of pile groups", *Sensors*, **18**(2), 476. https://doi.org/10.3390/s18020476.

Yuan, B.X., Liu, J.Y., Chen, W.W. and Xia, K.W. (2012), "Development of a robust stereo-PIV system for 3-D soil deformation measurement", *J. Test. Eval.*, **40**(2), 256-264. https://doi.org/10.1520/JTE103856.

Yuan, B.X., Sun, M., Xiong, L., Luo, Q.Z., Pradhan, S.P. and Li, H.Z. (2020), "Investigation of 3D deformation of transparent soil around a laterally loaded pile based on a hydraulic gradient model test", *J. Build. Eng.*, **28**(3), 101024. https://doi.org/10.1016/j.jobe.2019.101024.

Yuan, B.X., Xu, K., Wang, Y.X., Chen, R. and Luo, Q.Z. (2017), "Investigation of deflection of a laterally loaded pile and soil deformation using the PIV technique", *Int. J. Geomech.*, **17**(6), 04016138. https://doi.org/10.1061/(ASCE)GM.1943-5622.0000842.

Zhang, J.R., Jiang, T., Wang, X.C., Liu, C. and Huang, Z.Q. (2018), "Influences of drying and wetting cycles and compaction degree on strength of Yudong silt for subgrade and its prediction", *Adv. Civ. Eng.*, 1364186. https://doi.org/10.1155/2018/1364186.

Zhang, J.R., Niu, G., Li, X.C. and Sun, D.A. (2020), "Hydro-mechanical behavior of expansive soils with different dry densities over a wide suction range", *Acta Geotechnica*, **15**(1), 265-278. https://doi.org/10.1007/s11440-019-00874-y.

Zhang, J.R., Sun, D.A., Zhou, A.N. and Jiang, T. (2016), "Hydro-mechanical behaviour of expansive soils with different suctions and suction histories", *Can. Geotech. J.*, **53**(1), 1-13. https://doi.org/10.1139/cgj-2014-0366.

Zhang, T., Zhang, J.R., Jiang, T., Wang, X.C., Jia, H. and Wang, L.J. (2019), "SWCCs of silt in Yudong zone and its prediction under different drying-wetting cycle conditions", *Geotech. Geol. Eng.*, **37**(3), 1977-1986. https://doi.org/10.1007/s10706-018-0738-x.

Zhang, X., Liu, J.Y., Liu, M.L. (2019), "Experimental study on uplift behavior of group anchors in sand", *Geotech. Test. J.*, **43**(2), 687-702. https://doi.org/10.1520/GTJ20170430.

Zhou, A.N., Fan, Y., Cheng, W.C. and Zhang, J.R. (2019), "A fractal model to interpret porosity-dependent hyudraulic properties for unsaturated soils", *Adv. Civ. Eng.*, 3965803. https://doi.org/10.1155/2019/3965803.

CC